Convectively Forced Diurnal Gravity Waves in the Maritime Continent

JAMES H. RUPPERT JR., XINGCHAO CHEN, AND FUQING ZHANG

Department of Meteorology and Atmospheric Science, and Center for Advanced Data Assimilation and Predictability Techniques, The Pennsylvania State University, University Park, Pennsylvania

(Manuscript received 30 August 2019, in final form 24 December 2019)

ABSTRACT

Long-lived, zonally propagating diurnal rainfall disturbances are a highly pronounced and common feature in the Maritime Continent (MC). A recent study argues that these disturbances can be explained as diurnally phase-locked gravity waves. Here we explore the origins of these waves through regional cloud-permitting numerical model experiments. The gravity waves are reproduced and isolated in the model framework through the combined use of realistic geography and diurnally cyclic lateral boundary conditions representative of both characteristic easterly and westerly background zonal flow regimes. These flow regimes are characteristic of the Madden–Julian oscillation (MJO) suppressed and active phase in the MC, respectively. Tests are conducted wherein Borneo, Sumatra, or both islands and/or their orography are removed. These tests imply that the diurnal gravity waves are excited and maintained directly by latent heating from the vigorous mesoscale convective systems (MCSs) that form nocturnally in both Borneo and Sumatra. Removing orography has only a secondary impact on both the MCSs and the gravity waves, implying that it is not critical to these waves. We therefore hypothesize that diurnal gravity waves are fundamentally driven by mesoscale organized deep convection, and are only sensitive to orography to the measure that the convection is affected by the orography and its mesoscale flows. Factor separation further reveals that the nonlinear interaction of synchronized diurnal cycles in Sumatra and Borneo slightly amplifies this gravity wave mode compared to if either island existed in isolation. This nonlinear feedback appears most prominently at longitudes directly between the two islands.

1. Introduction

The diurnal cycle is the leading mode of rainfall variability in many regions of the world, particularly in tropical islands and in continental regions adjacent to warm waters (Dai 2001; Ohsawa et al. 2001; Yang and Slingo 2001; Neale and Slingo 2003; Nesbitt and Zipser 2003; Yang and Smith 2006; Kikuchi and Wang 2008; Johnson 2011; Ruppert et al. 2013; Chen et al. 2016). The Maritime Continent (MC) is exemplary for this, where prominent land–sea breeze circulations diurnally trigger deep moist convection each afternoon, which in turn grows upscale into vigorous mesoscale convective systems (MCSs) (Houze et al. 1981; Johnson and Priegnitz 1981; Johnson 1982; Mapes and Houze 1993). These MCSs often propagate offshore overnight, enduring well into the next day (Mori et al. 2004; Yamanaka et al. 2018). A prevalence of long-lived nocturnally offshore-propagating rainfall signatures has been noted in many regions of the world, though the root driver of this propagation remains unclear. The present study investigates this phenomenon in the context of the MC.

Long-lived eastward-propagating nocturnal MCSs routinely develop from afternoon cellular convection in the Rockies during the warm season (Carbone et al. 2002; Carbone and Tuttle 2008). These MCSs are the predominant driver of summertime rainfall in the United States between the Rockies and Appalachians. An analogous phenomenon manifests in continental China east of the Tibetan Plateau during the warm season (Wang et al. 2004; Bao et al. 2011), and likewise for many other continental regions downstream of mountain ranges (e.g., Laing et al. 2008). Many studies have argued that a key driver of this phenomenon is the mountain–plains solenoidal circulation (Carbone and Tuttle 2008; Huang et al. 2010; Sun and Zhang 2012; Bao and Zhang 2013), and the nocturnal low-level jet in the case of the United States (Stensrud 1996; Trier et al. 2014). These mechanisms conspire to promote nocturnal low-level convergence, moistening, and destabilization, and hence provide

Corresponding author: James H. Ruppert Jr., jruppert.jr@gmail.com

DOI: 10.1175/JAS-D-19-0236.1

explanations for the triggering and maintenance of these MCSs, though not their propagation.

Yet in other regions, nocturnal propagating convective systems exist both without low-level jets and without continuous orographic forcing, as exemplified by the many examples of offshore-propagating nocturnal systems: in the Tiwi Islands (Carbone et al. 2000); the Panama Bight region (Mapes et al. 2003a,b; Warner et al. 2003), the South China Sea (Aves and Johnson 2008; Chen et al. 2016), the Bay of Bengal (Yang and Slingo 2001; Zuidema 2003), and many of the islands of the MC (Mori et al. 2004; Ichikawa and Yasunari 2006, 2008; Sakurai et al. 2009; Vincent and Lane 2016). This raises the following question: What is common between the coastal and continental regimes? One commonality is a clear *nocturnal* preference for MCS activity (Nesbitt and Zipser 2003). Largely through two concurrent mechanisms, the diurnal change in atmospheric radiative heating conspires to favor nocturnal organized deep convection (Gray and Jacobson 1977; Randall et al. 1991; Ruppert and Hohenegger 2018). While this argument has primarily been invoked to explain nocturnal–early morning rainfall over oceans (Yang and Slingo 2001; Yang and Smith 2006), its potential role over land has also been implicated (Zhang et al. 2018).

A striking commonality between both the coastal and continental regimes of propagating diurnal MCSs is a horizontal phase speed of $\sim$15–20 m s^{-1} (Mapes et al. 2003b; Carbone and Tuttle 2008). This phase speed and assessment of vertical wind profiles rules out the role of both basic advection and synoptic-scale Rossby waves. It is also too fast to be explained by convective cold pools; for density currents to propagate this fast requires associated temperature anomalies exceeding $\sim$10 K (Markowski and Richardson 2010). Cold pools of this magnitude are rare, even in the continental regime (Trier et al. 2014). While there is evidence of slower propagation linked to both cold pools and land-breeze density currents embedded within these systems (i.e., $\sim$3–8 m s^{-1}) (Houze et al. 1981; Johnson and Bresch 1991; Sakurai et al. 2009; Fujita et al. 2011; Chen et al. 2016; Coppin and Bellon 2019; Ruppert and Zhang 2019, RZ19 henceforth), the faster propagation requires another explanation, which is where gravity waves come in (Tripoli and Cotton 1989; Yang and Slingo 2001; Mapes et al. 2003b; Ichikawa and Yasunari 2007; RZ19).

There is growing support for a gravity wave–convection interaction mechanism for explaining these nocturnal propagating MCSs. Key to their observed phase speeds is the development of high-order gravity wave packets in response to the prominent stratiform heating structure in organized convection (Mapes et al. 2006; Tulich et al. 2007; Tulich and Mapes 2008; Love et al. 2011). These gravity wave modes are characterized by vertical wavelengths smaller than the depth of the troposphere, and accordingly, phase speeds in the range $\sim$15–20 m s^{-1} (Nicholls et al. 1991; Mapes 1993). These modes have been found to both destabilize and moisten the lower troposphere ahead of the MCS, in turn driving its discrete forward propagation via the triggering of new convective cells (Mapes 2000; Fovell et al. 2006; Kuang 2008; Tulich and Mapes 2008). This mechanism or similar ones have been invoked to explain MCS evolution and propagation in both the coastal and continental regime (Fovell et al. 2006; Love et al. 2011; Pritchard et al. 2011; Vincent and Lane 2016; Coppin and Bellon 2019).

What is the role of orography in this offshore propagation? In the case of the Panama Bight region, Mapes et al. (2003b) argued that elevated terrain excites a gravity wave, which in turn explains the offshore propagation as follows: solar heating of the boundary layer along a sloped surface creates a localized buoyancy anomaly, which excites a gravity wave that couples with rainfall as it propagates away. Yet, topography varies greatly from region to region, and may not be critical to the offshore propagation or the generation of gravity waves, which may instead be continuously excited by organized convection in accordance with the stratiform-heating mechanism described above. We examine this hypothesis here. Specifically, RZ19 hypothesized that the zonally propagating diurnal MCSs in the MC can be explained as a diurnal gravity wave mode excited by and coupled with vigorous latent heating.

Zonally propagating diurnal convection in the MC is likely especially unique owing to the particular distribution of land and sea there. These systems typically propagate at a phase speed of $\sim$17 m s^{-1}, and often endure over multiple days (Ichikawa and Yasunari 2007; RZ19). RZ19 provides evidence supporting the interpretation of these disturbances as convectively coupled gravity waves. An especially intriguing consequence of the MC's geometry is as follows. Since the distance between Borneo and Sumatra is $\sim$1500 km, the 17 m s^{-1} phase speed of these systems results in their being situated favorably to couple with diurnal convection over both islands over a 2-day sequence (RZ19). Hence, these diurnal gravity waves are diurnally phase-locked. RZ19 hypothesized that the synchronized diurnal forcing of these two islands drives a stronger gravity wave response than would occur if only one island existed in isolation. We test this hypothesis herein.

The direction of their zonal propagation is strongly controlled by the background low-level flow direction.

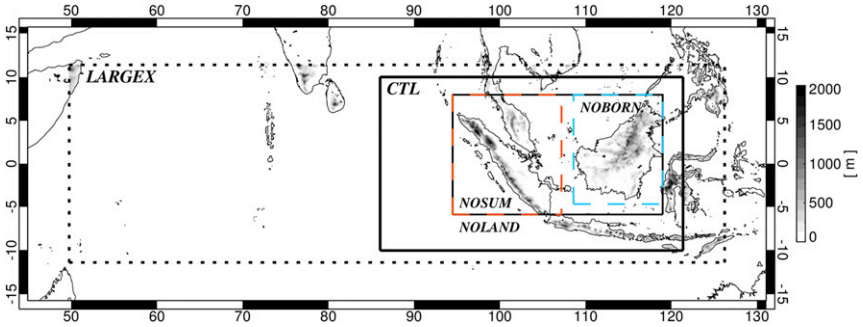

FIG. 1. Model simulation domains. All simulations use the CTL domain, except LARGEX. The rectangles labeled NOLAND, NOSUM, and NOBORN indicate the regions where orography and/or surface type are modified for the corresponding experiments. Topography is shaded (only inside LARGEX domain) according to the color bar.

Hence, the passage of the Madden–Julian oscillation (MJO) (Madden and Julian 1972) strongly influences this direction (Ichikawa and Yasunari 2007; RZ19). Specifically, the gravity waves propagate westward under easterly flow at 850 hPa, or during the local suppressed phase of the MJO when the active phase is situated in the central Indian Ocean. Conversely, the disturbances propagate eastward under westerly flow in association with the MJO active phase. Understanding the nature and role of these propagating disturbances, and their sensitivity to the background wind, may ultimately improve our understanding of the complex interaction between the MJO and the MC (Feng et al. 2015; Gonzalez and Jiang 2017; Sakaeda et al. 2017; Zhang and Ling 2017).

Here we examine the origins and sensitivities of the diurnally phase-locked gravity waves in the MC through semi-idealized cloud-permitting numerical model experiments. Realistic geography is imposed in these experiments, while the lateral boundary conditions are semi-idealized by repeating a diurnal composite calculated from a regime of interest, following the technique of several past studies (Trier et al. 2010; Sun and Zhang 2012; Chen et al. 2016). We conduct a series of sensitivity tests modifying the islands or their existence in order to test the study objectives, which are as follows:

1) To assess the dynamic origins of diurnal gravity waves in the MC region and the specific role of orography for these waves.
2) To quantify the nonlinear response to the synchronized diurnal forcing of Borneo and Sumatra.

2. Methodology

The regional cloud-permitting numerical model framework of this study is based on that of Wang et al. (2015), who invoked the Weather Research and Forecasting (WRF) Model, version 3.4.1 (Skamarock et al. 2008), to conduct a 2-month simulation over a region covering both the Indian Ocean and MC from 1 October to 15 December. This period spans the primary observing period of the 2011/12 Dynamics of the MJO (DYNAMO) field campaign (Yoneyama et al. 2013), which captured two MJO events. This simulation framework has been employed to study the MJO (Zhang et al. 2017; Chen et al. 2018; Chen and Zhang 2019) and other convectively coupled modes (Ying and Zhang 2017). More recently, RZ19 employed the model setup to investigate the diurnal gravity waves in the MC that are the subject of this study.

This study invokes a virtually identical numerical model setup to that of RZ19 and Wang et al. (2015), but using a different model domain (Fig. 1) and forced using modified lateral boundary conditions, as described below. The model domain is reduced in size since our focus is on the MC. The model grid is discretized with 9-km horizontal spacing, with 45 stretched vertical levels and a top at 20 hPa. The vertical grid includes 9 levels in the lowest 1.2 km, where spacing Δz ranges from ~50 to 200 m; Δz increases to 800 m by $z \approx 15$ km, and peaks at 1000 m for $z \approx 20$ km. This grid spacing adequately captures the mesoscale convective motions and their coupling with the large scale, although it does not properly resolve individual convective elements (Chen et al. 2018). The two-moment WRF microphysics scheme is invoked. Radiation is treated using the RRTMG longwave scheme (Iacono et al. 2008) and the updated Goddard shortwave model (Chou and Suarez 1994; Shi et al. 2010). The surface is treated with Noah physics and the ocean surface skin temperature scheme of Zeng and Beljaars (2005). Refer to Wang et al. (2015) for additional details.

RZ19 used a threshold of low-pass-filtered zonal flow at 850 hPa to identify regimes of daily mean easterly and

TABLE 1. Model simulations of the study. All sensitivity tests are identical to CTL, except for the noted changes.

Easterly flow regime	
CTL	Realistic geography and forcing
CONSTBC	BCs fixed to daily mean
HIRES	3-km horizontal grid spacing
LARGEX	Domain expanded to include entire Indian Ocean
NOSUM	Sumatra removed
NOBORN	Borneo removed
NOLAND	Sumatra and Borneo removed
NOOROG	Orography of Sumatra and Borneo flattened
NODC	Daily mean TOA insolation
Westerly flow regime	
W_CTL	Realistic geography and forcing
W_NOOROG	As in NOOROG
W_NOLAND	As in NOLAND

westerly flow over the MC, which neatly distinguishes regimes of westward- and eastward-propagating diurnal gravity waves, respectively (cf. Fig. 2 of RZ19). We use these two regimes here. The easterly regime (13–30 October 2011, inclusive) closely corresponds with the suppressed phase of the MJO in the MC, as during this period the MJO convective envelope was situated in the Indian Ocean. This regime is also analogous to an active northeasterly monsoon period in the MC (Houze et al. 1981; Johnson and Priegnitz 1981). The westerly regime (1–10 October and 1–10 November) is characteristic of the MJO active phase in the MC. The majority of the study relies on the easterly regime, with some analysis repeated for the westerly regime to demonstrate robustness.

Special lateral boundary conditions are imposed to simulate the diurnal gravity waves and isolate them from other variability. Namely, using the above two regimes, we generate diurnally cyclic boundary conditions by averaging 6-hourly reanalysis data in time as a function of hour, yielding a single diurnal composite for both. For example, the composite cyclic boundary conditions at 0000 UTC for the easterly regime represent the average of the reanalysis at all 0000 UTC samples from 13 to 30 October 2011, and so forth. This procedure is applied to all meteorological input variables. The European Centre for Medium-Range Weather Forecasts (ECMWF) interim reanalysis (ERA-Interim) is invoked for these boundary conditions (Dee et al. 2011).

All of the simulations of the study are summarized in Table 1. A control simulation (CTL) is conducted on the domain shown in Fig. 1 using the easterly regime diurnal composite repeated in time for 30 days to assess its evolution. The simulation reaches a statistically steady state in <5 days and is qualitatively unchanged thereafter (Fig. 3; only the first 10 days are shown). We therefore focus on the first 10 days of this simulation, and run all other tests for only 10 days. All analysis is based on hourly model output. A control test is also conducted for the westerly regime, W_CTL (all tests for this regime have the prefix "W_" in their name).

Several sensitivity tests are conducted to address the study objectives. Each test is identical to CTL but for the modification(s) indicated. To assess if the diurnal gravity waves are influenced by external forcing outside the model domain, the test CONSTBC is conducted where the lateral boundary conditions are fixed to the composite time-mean of 13–30 October. In the next four tests, only the lower boundary condition is modified, keeping the lateral boundary conditions as in CTL. For the tests NOSUM, NOBORN, and NOLAND, all land (and orography) is removed in the corresponding annotated squares in Fig. 1 by replacing it with ocean in all pertinent quantities. In NOOROG, land is retained but the orography is flattened in the rectangle annotated NOLAND. The initial atmospheric state is also modified in these tests to account for the removal or orography: the mass, moisture, and flow fields of columns with flattened orography are replaced throughout the vertical by spatial averages over ocean points that fall within the corresponding rectangle. We repeat the orographic and land removal tests for the westerly regime: W_NOOROG and W_NOLAND.

Next, to clearly identify the specific role of diurnal forcing, solar forcing is fixed to its daily mean in the test NODC, as in several past studies (Mapes et al. 2003b; Hagos et al. 2016; Ruppert 2016; Ruppert and Johnson 2016). We do so by matching solar forcing to its insolation-weighted daily mean, following Cronin (2014). Namely, the solar zenith angle is set to 48.19° and the solar constant is set to 659 $\mathrm{W\,m^{-2}}$ in the solar radiation scheme, yielding a constant TOA insolation of 429 $\mathrm{W\,m^{-2}}$ over the MC, which matches the daily average of that in CTL. Moreover, this approach yields a better match of atmospheric solar heating between CTL and NODC than other approaches to fix insolation (Cronin 2014). The lateral boundary conditions are also fixed to the daily mean in NODC, as in CONSTBC.

Last, two sensitivity tests are conducted to assess sensitivities to model and domain specifications. To assess the sensitivity to grid spacing, a high-resolution test (HIRES) is conducted with 3-km horizontal grid spacing and 55 vertical levels. To assess the sensitivity to domain size, the test LARGEX is conducted on a domain that is greatly expanded in longitude (Fig. 1). Several other domain-size tests were conducted with the lateral

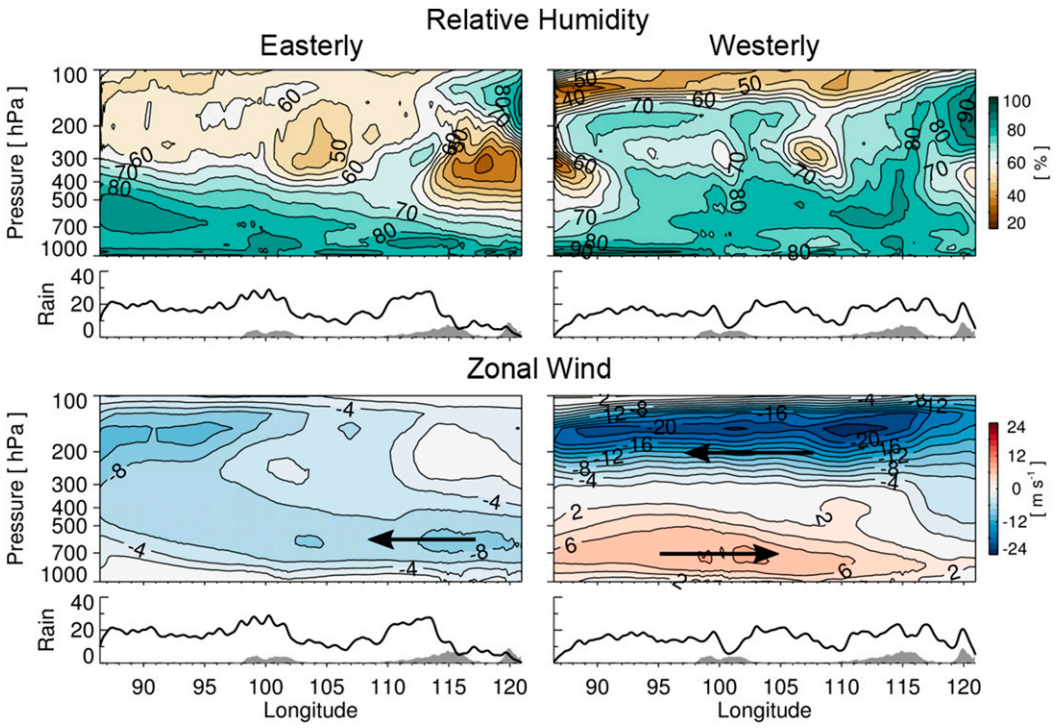

FIG. 2. Zonal cross sections (pressure–longitude) averaged from 3°S to 3°N and over days 5–10 in (left) the easterly regime simulation (13–30 Oct 2011; CTL) and (right) westerly regime simulation (1–10 Oct and 1–10 Nov; W_CTL). Shown are (top) relative humidity and (bottom) zonal wind u, with rainfall (mm day^{-1}; black line) and topography (shading; not to any scale) in lower panels of each row. Rainfall is zonally smoothed using a Gaussian filter with a two-point standard deviation.

boundaries pushed farther away from the MC. In all such tests, the diurnal gravity waves in the MC appear qualitatively consistently, and hence these other tests are left out for brevity.

3. Analysis

a. Character and origins of diurnal gravity waves

The mean states of the two control simulations, CTL and W_CTL, are depicted through time-mean cross sections averaged from 3°S to 3°N (Fig. 2). The dramatic distinctions between these regimes are clear, and are consistent with the local life cycle of the MJO. The general character of these regimes is also consistent with both reanalysis and the longer continuous simulations of RZ19 (their Fig. 3). In the easterly regime, easterly flow prevails throughout the column, with high values of humidity confined to the lower–midtroposphere over much of the MC. The easterlies decrease in strength with height over the MC and weaken over the Indian Ocean in the lower troposphere, consistent with low-level convergence over the Indian Ocean (~93°E) in connection with the MJO convective envelope. The mean humidity field is characterized by a moist boundary layer and lower free troposphere, with moisture substantially increasing toward the western edge of the domain in connection with this convergent flow. This zonal flow pattern closely matches that in reanalysis for the same composite time period (Fig. 3a of RZ19). It is possible that the high humidity near the western edge of the model domain is a moist bias due to the constant daily mean forcing imposed by the idealized boundary conditions, given that it does not appear in simulations with time-varying boundary conditions (Fig. 3e of RZ19). Rainfall exhibits two prominent peaks up to ~30 mm day^{-1} associated with the two islands, with a weaker third peak over the Indian Ocean linked to the convergent flow there.

The westerly regime, in contrast, is characterized by a much moister free troposphere, with strong westerlies from the surface up to midlevels, which weaken toward the east (Fig. 2). This strong low-level westerly flow and convergence over the eastern MC is consistent with the active phase of the MJO. While there is rainfall of ~20 mm day^{-1} over much of the region, there are not as clear of peaks over the islands as compared to the easterly regime. This difference may owe to suppressed shortwave surface heating due to greater cloud cover in

this regime (Oh et al. 2012; Hagos et al. 2016; Sakaeda et al. 2017; Zhang and Ling 2017; Ling et al. 2019). This regime is nonetheless characterized by prominent diurnal variation of convection, as described later.

Hovmöller diagrams for CTL (the easterly regime) reveal very prominent westward-propagating disturbances, consistent with those described by Ichikawa and Yasunari (2007) and RZ19 under background easterly flow (Fig. 3). The disturbances are characterized by two prominent daily rainfall peaks that propagate westward over and offshore from both Borneo and Sumatra. As will be demonstrated, these two diurnal peaks are linked through their coupling with a propagating diurnal gravity wave. This gravity wave mode appears very prominently beginning on the first or second simulated day, and remains qualitatively similar throughout the 10-day period shown. The wave becomes slightly stronger over the 10-day period in terms of rainfall magnitude, as the zonal easterly flow strengthens by ~1–2 $m\,s^{-1}$. The exact cause for this subtle zonal flow increase remains uncertain, though it is likely tied to the idealized nature of the study, as it is similarly apparent in the other simulations of this regime (Fig. 3). A slight day-to-day increase of rainfall between the western domain edge and ~100°E is also apparent in CTL, likely owing to increasing moisture in this region in connection with persistent low-level convergence (Fig. 2). These subtle changes over the 10-day period do not affect the qualitative character of the gravity wave mode.

The mean gravity wave structure is depicted next through diurnal composites of rainfall and zonal wind with the mean removed u' at 150 hPa (Fig. 4), which are calculated by averaging from days 5–10 as a function of local time (LT). The composite gravity waves in CTL exhibit a westward phase speed of ~18 $m\,s^{-1}$ based on u'. This u' signal implies upper-level divergence roughly collocated with enhanced rainfall. The two prominent rainfall maxima propagate more slowly than the u' signal (~11 $m\,s^{-1}$), and hence appear disconnected in time between the islands (i.e., ~105°–107°E). Nonetheless, the space–time continuity of the u' signal implies that the diurnal gravity wave coupled to this rainfall signal is continuous between the diurnal convective cycles of both islands. This is consistent with the findings of RZ19. This relationship implies that the overriding gravity wave likely orchestrates the development of sequential rainfall events along its trajectory (i.e., via discrete propagation; Fovell et al. 2006; Tulich et al. 2007). The phase speed of ~18 $m\,s^{-1}$ is ~1 $m\,s^{-1}$ faster than that noted by RZ19. This difference may owe to slightly stronger background easterly low-level flow in this simulation owing to the special boundary conditions imposed (e.g., compare Fig. 2 with Fig. 3a of RZ19). Nonetheless, these gravity waves are highly consistent with those of RZ19—namely, they are diurnally phase-locked, in that they propagate the distance between Borneo and Sumatra in one diurnal cycle and couple with the diurnal convective cycles over both islands.

The signals in both rainfall and u' in CTL appear to originate in the vicinity of eastern Borneo (~115°E), with rainfall strongly increasing starting around 1600 LT (Fig. 4). This Borneo rainfall system peaks around midnight, continues to migrate westward through morning, and connects with a secondary rainfall maximum around noon the next day in the Karimata Strait (~107°E; the sea between Borneo and Sumatra). Rainfall also begins increasing around noon in the eastern Sumatra and Malay Peninsula region, intensifying throughout the afternoon, and again peaking around midnight over Sumatra's steepest slopes and the coastline (~100°E). This rainfall system then persists for at least another 12 h as it continues westward. Comparison with both TRMM rainfall and more realistic WRF simulations suggests that this diurnal evolution is realistic (Figs. 2a and 4a,c of RZ19).

Horizontal maps of diurnal composite 150-hPa u' and virtual potential temperature with the time-mean and time-varying zonal mean removed θ_v^* are shown in Fig. 5. Composite total wind and rainfall are overlaid. With smoothing applied, these fields emphasize mesoscale–synoptic-scale signals rather than those of individual thunderstorms. As in Fig. 4, a regular wavelike pattern in u' and θ_v^* extends well across both Borneo and Sumatra in the zonal direction, with the wave patterns also extending at least ~10° in latitude. The maps also reveal an important gravity wave signature: divergent zonal flow peaks over areas of strongest rainfall (Fig. 5b), with associated peaks in θ_v^* (Fig. 5a) shifted 90° in phase relative to the u' signal. This out-of-phase wave signal may project onto the equatorially trapped $n = 1$ westward inertio-gravity wave (e.g., Kiladis et al. 2009), though it is perhaps more accurately described as mesoscale in nature, given that it assumes the geometry of the islands. A clear example of this is the northwest–southeast orientation of its signal offshore (southwest) of Sumatra.

To examine this gravity wave mode and its interaction with deep convection more closely, diurnal composite cross sections are provided for vertical motion w, u', and θ_v^* (Fig. 6). The qualitative consistency of these cross sections with those of RZ19 corroborates that this semi-idealized framework realistically reproduces these diurnal gravity waves. Two very prominent mesoscale updrafts appear with an approximately synchronized

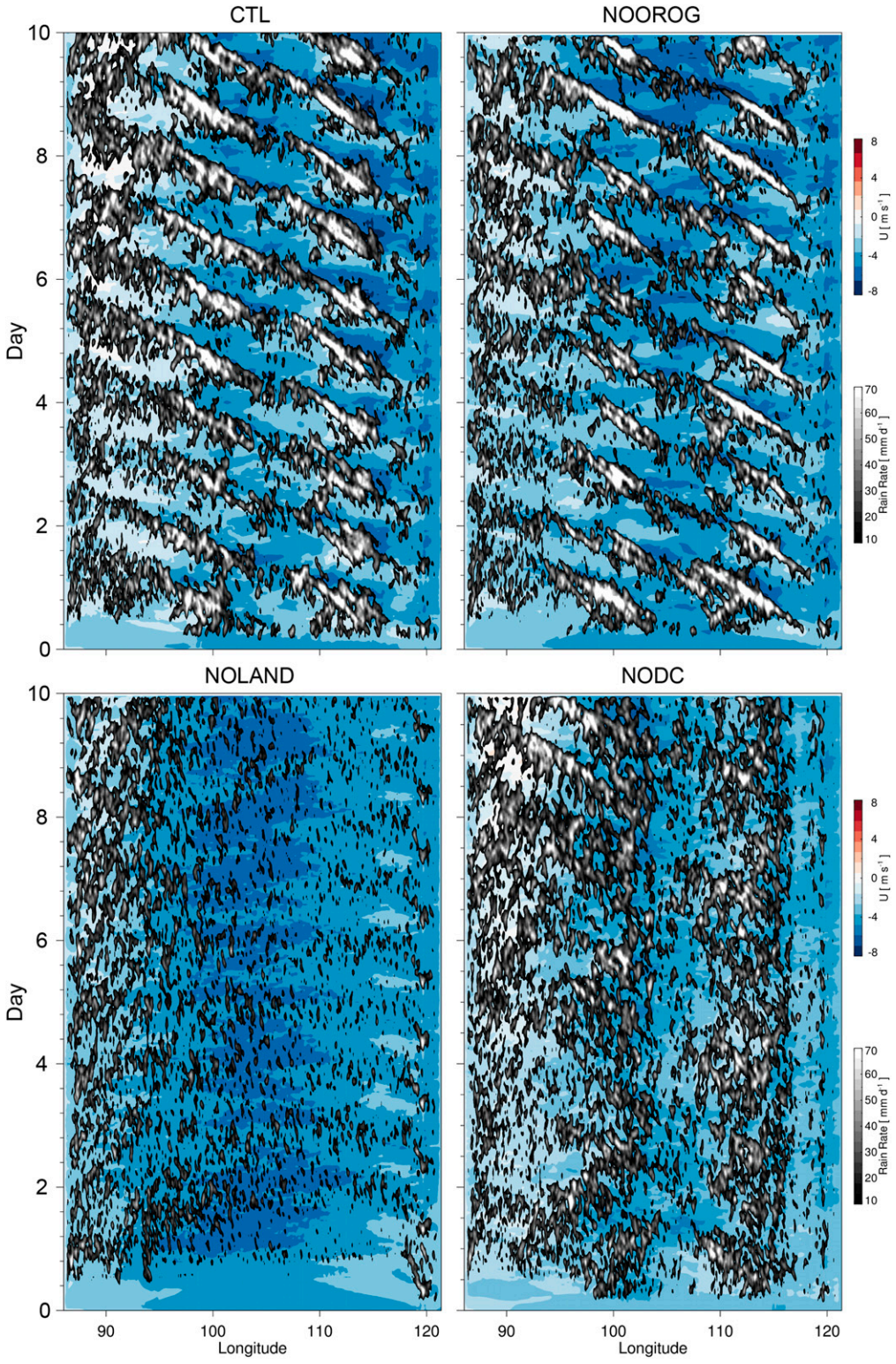

FIG. 3. Zonal Hovmöller diagrams averaged from 3°S to 3°N with rainfall (grayscale shading) and 850-hPa zonal wind u (red to blue shading).

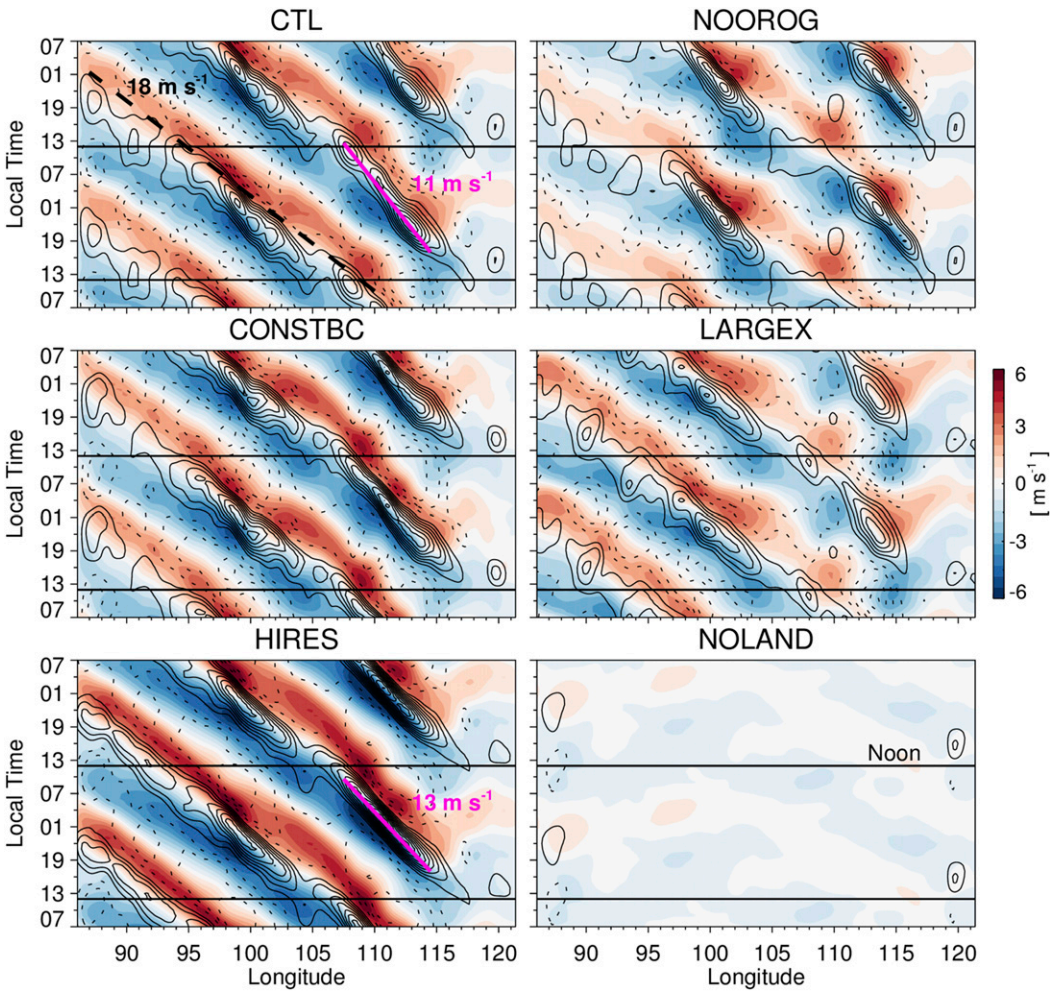

FIG. 4. Diurnal composite zonal Hovmöller diagrams averaged from 3°S to 3°N for days 5–10, with diurnal-anomaly rainfall r' (contoured every 6 mm day^{-1}) and 150-hPa u with the time-mean subtracted u' (shaded). Variables are smoothed using Gaussian filters with standard deviations of 0.5° in longitude and 1 h in time. Phase speed lines of 18 (black dashed) and 11 and 13 m s^{-1} (magenta solid) are depicted.

evolution over the Borneo and Sumatra regions beginning around 1900 LT, indicative of evening or nocturnal MCS development likely triggered by the land breeze (Fig. 6a) (Houze et al. 1981; Johnson 1982; RZ19). The associated maxima in w are top-heavy, with peaks in the upper troposphere extending beyond 200 hPa, consistent with a large proportion of stratiform precipitation within the MCSs (Houze et al. 1981). These systems are characterized by peak rainfall through the midnight period, from 2200 to 0100 LT. Tracking the rainfall peaks through time indicates an apparent propagation of ~11 m s^{-1}, in contrast to the prominent upper-level anomalies in u' and θ_v^*, which propagate ~7 m s^{-1} faster (Figs. 4 and 6b,c).

As in RZ19, u' and θ_v^* exhibit very prominent upward- and downward-tilted rays that appear to radiate westward away from a source in the mid- to upper troposphere (Figs. 6b,c). These signatures are in quadrature, consistent with gravity wave energy excited by a westward-moving tropospheric heat source (Takayabu et al. 1996; Kiladis et al. 2009). These signatures are strongest over the two main MCSs of Borneo and Sumatra from 2200 to 0700 LT, with upper-level divergence situated near the strongest rainfall, as in the maps in Fig. 5. This relationship exemplifies the strong coupling between the gravity wave and the deep convection. Furthermore, these relationships support the hypothesis of RZ19 that these diurnal gravity waves are excited and maintained primarily by latent heating from the vigorous diurnal MCSs of Borneo and Sumatra (Raymond 1984; Tripoli and Cotton 1989).

The sensitivity test HIRES indicates that these gravity waves are qualitatively insensitive to the selection of horizontal resolution (Fig. 4): namely, the gravity waves

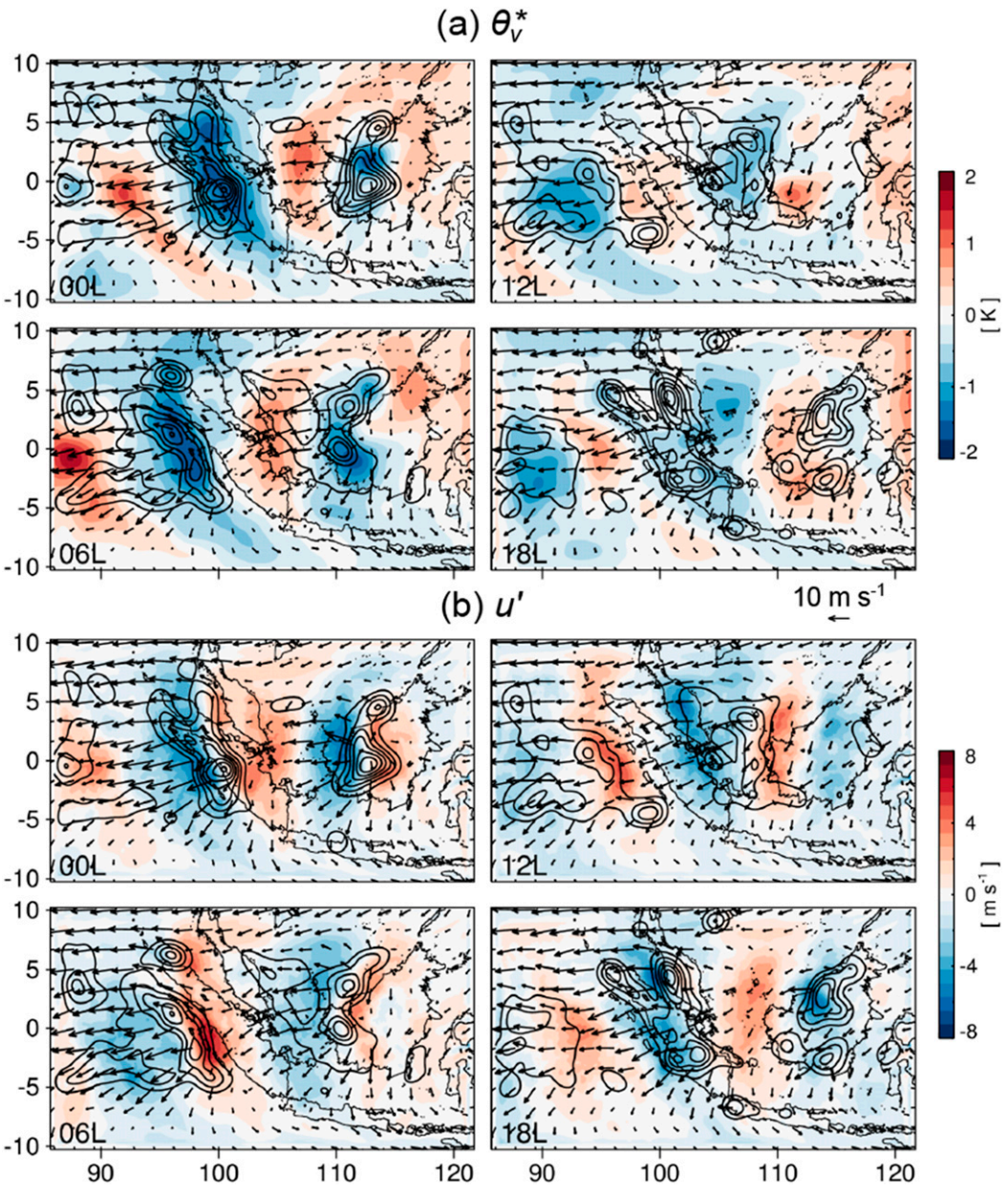

FIG. 5. Diurnal composite maps for days 5–10 of 150-hPa (a) virtual potential temperature with the time-mean and diurnally varying zonal-mean removed θ_v^* (shaded; K) and (b) u' (m s^{-1}), with total wind (vectors) and rainfall (contoured every 15 mm day^{-1}). Values of u', θ_v^*, and rainfall are horizontally smoothed using a Gaussian filter with a seven-point standard deviation.

appear in HIRES with very similar westward phase speed and positioning. With higher resolution, however, both the associated rainfall and zonal flow anomalies reach greater amplitude. The MCSs in HIRES also exhibit faster westward motion, by ~2 m s^{-1}. RZ19 found that the westward motion of these MCSs is consistent with density current theory based on estimated cold pool strength. Following this argument, faster MCS motion in HIRES likely owes to stronger precipitation-driven cold pools in connection with more intense rainfall. More generally, this sensitivity emphasizes that the 9-km horizontal grid mesh of CTL underresolves some features of the moist convection, although the 9-km grid nonetheless captures the convection–gravity wave coupling with qualitative consistency to the 3-km grid. The sensitivity test LARGEX further indicates that the westward phase speed and positioning of gravity waves is qualitatively insensitive to the exact locations of the lateral domain boundaries.

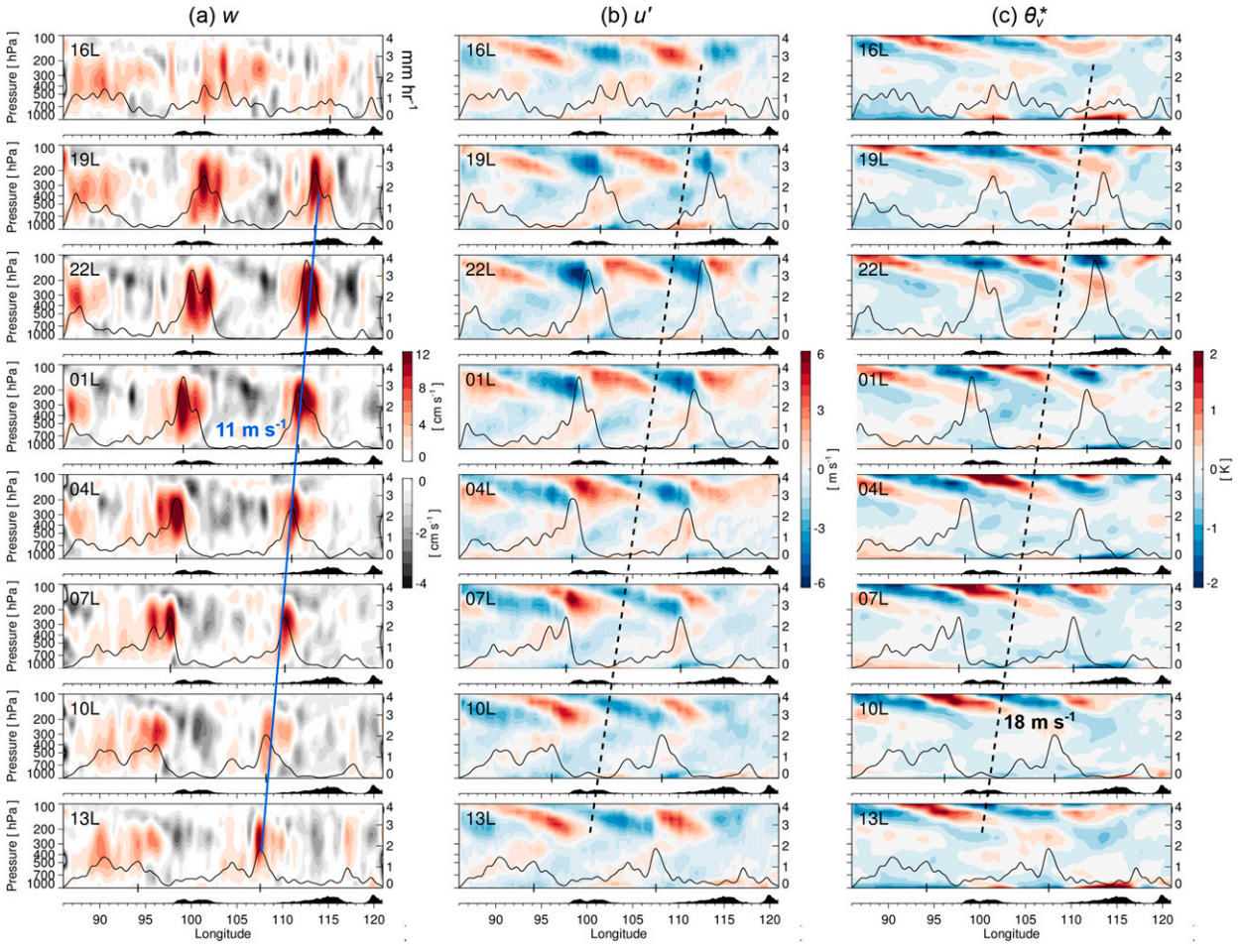

FIG. 6. Diurnal composite zonal cross sections averaged from 3°S to 3°N in CTL for days 5–10, including (a) vertical motion w, (b) u', and (c) θ_v^*. Rainfall is overlaid (mm h^{-1}; according to the right ordinate), with hashes along the abscissa marking local maxima. Topography is depicted beneath each panel (not to any scale). Values of w (θ_v^*) is zonally smoothed using a Gaussian filter with three- (two-) point standard deviation. Phase speed lines of 11 (blue solid) and 18 m s^{-1} (black dashed) are depicted.

This relative insensitivity to the locations of the boundary edges implies that the waves are generated internally within the model domain.

The remaining sensitivity tests provide deeper insights into the origins of the gravity waves (Figs. 3 and 4). The very close match between CTL and CONSTBC indicates that the waves are not sensitive to the time-varying lateral boundary conditions, thereby confirming that they are excited by local diurnal forcing within the model domain. This is consistent with the general insensitivity to domain edge location as indicated by LARGEX. Comparing CTL with NOLAND[1] reveals that land–sea contrast due to the islands is of first-order importance for the gravity waves (Figs. 3 and 4). Namely, owing to this land–sea contrast, the diurnal land–sea breeze systems trigger vigorous nocturnal MCSs (Houze et al. 1981; Johnson and Kriete 1982; Mori et al. 2004), which in turn are critical to exciting the gravity waves. The critical role of the deep convection in exciting these waves is corroborated by the westward-tilted rays in u' and θ_v^*, indicative of vertical propagation of gravity wave energy in response to a westward-moving heat source (Figs. 6b,c). In the test NODC, there is no diurnal variability, by design, and hence no diurnal gravity waves (Fig. 3). The variance apparent in this test is unrelated to the diurnal cycle, and owes instead to modes that develop internally (not explored here). It is intriguing to note, nonetheless, that rainfall in NODC is much greater than in

[1] While virtually all trace of the diurnal gravity waves is absent in this test, some remains. This remnant signal is due to diurnal forcing from the very mountainous island of Sulawesi located east of Borneo (just inside the eastern edge of the model domain), which is not removed in this test.

NOLAND, implying that basic-state forcing due to islands, in the absence of diurnal forcing, also plays a vital role in island rainfall enhancement (Qian 2008; Cronin et al. 2015). This subject is explored in a separate study by the authors (Ruppert and Chen 2020).

Removing the orography of both island regions (NOOROG) has only a second-order impact on the gravity waves compared to fully removing the islands (Figs. 3 and 4). The individual propagating rainfall features in NOOROG are characterized by shorter lifetimes, however, as exemplified in particular by weaker rainfall and upper-level signatures in u' over the Karimata Strait and to the west of Sumatra. We suggest two potential explanations for this secondary orographic influence. The first is the asymmetry in the land–sea breeze system caused by topography. The theoretical study of Qian et al. (2012) indicates that sloped terrain near the coastline can amplify the nocturnal land-breeze density current and its offshore propagation rate, as follows. The sloped terrain blocks the inland penetration of the daytime sea breeze, causing a cold pool to develop near the coastline. This cold pool later becomes the nocturnal land breeze, which is then further strengthened by nocturnal cooling. Chen et al. (2016) found that the diurnal offshore rainfall propagation near coastal southern China can be explained by this process. It is plausible that this orographic land-breeze amplification mechanism plays a role in promoting stronger offshore convective triggering, and in consequence, a stronger gravity wave through its coupling with convection.

The second potential explanation for orographic enhancement of the gravity waves offshore is the role of diurnal heating and cooling of sloped terrain and the specific gravity wave response to this forcing, as proposed by Mapes et al. (2003b). They argued that this orographically generated gravity wave mechanism is vital to the offshore-propagating diurnal rainfall signals in the Panama Bight region. While it is possible that this orographic gravity wave mechanism is important to explaining these differences between the rainfall signals of CTL and NOOROG, these results nonetheless demonstrate that this mechanism is not vital to the diurnal gravity waves in the MC.

This result stands in contrast to the experiments of Mapes et al. (2003b), wherein they found that removing orography completely removed the diurnal gravity waves. A major difference between the Panama Bight region and the MC is that the Andes Mountains, given their extreme nature, likely play a much more critical role in determining the mesoscale–synoptic-scale circulation in that region. When Mapes et al. removed orography, this indeed also dramatically altered the lower-tropospheric flow impinging on the Andes, in turn causing substantial changes to rainfall across the basin. In our study, in contrast, removing orography does not dramatically affect the mean flow, nor mean rainfall (Fig. 3). An additional potential contributing factor to this distinct finding is the role of higher convective instability in the MC region, which may allow for more easy triggering of convection. This possibility is worth investigating in the future.

Given the above arguments, we propose the following hypothesis that future work may test: offshore-propagating diurnal gravity waves and coupled rainfall signatures are fundamentally triggered by organized deep convection, and are only sensitive to orography to the extent that deep convection is sensitive to orographically driven mesoscale flows. The link between orography, mesoscale flows, and moist convection may manifest through one or several distinct mechanisms, including the two examples described above. According to this hypothesis, however, organized deep moist convection, rather than orography, is viewed as the critical driving force that excites the diurnal gravity waves.

Next, the simulations conducted for the westerly regime are examined. The results of both Ichikawa and Yasunari (2007) and RZ19 suggest that these diurnal modes propagate eastward under westerly flow. A potentially important distinction of this regime from the easterly flow regime is much stronger vertical shear, with easterly flow in the upper troposphere and westerlies in the lower troposphere (Fig. 2) (RZ19). The influence of this distinction on the waves and the convection they couple with is assessed next.

Hovmöller diagrams of rainfall and 850-hPa flow for W_CTL reveal very prominent eastward-propagating diurnal modes (Fig. 7). These modes are indeed more prominent than in the corresponding composite of RZ19. Higher-amplitude diurnal variability is a common effect when diurnal composite lateral boundary conditions are imposed, and likely owes to the effective filtering of variability at longer time scales (Sun and Zhang 2012; Trier et al. 2014; Chen et al. 2016, 2017). Diurnal composites for these tests are provided in Fig. 8, with u' shown at 400 instead of 150 hPa. We choose this level because convection peaks at a lower level in this regime, and hence so does divergence, as compared to the easterly flow regime (shown later).

These modes exhibit an eastward phase speed of $\sim 14\,\mathrm{m\,s^{-1}}$, with discontinuous propagation between Sumatra and Borneo (Fig. 8). Convection first intensifies around 1900 LT in the vicinity of Sumatra (~100°E), propagating eastward into central Borneo (~114°E) through the early morning hours. But convection is unsupported over Borneo at these hours, and hence as

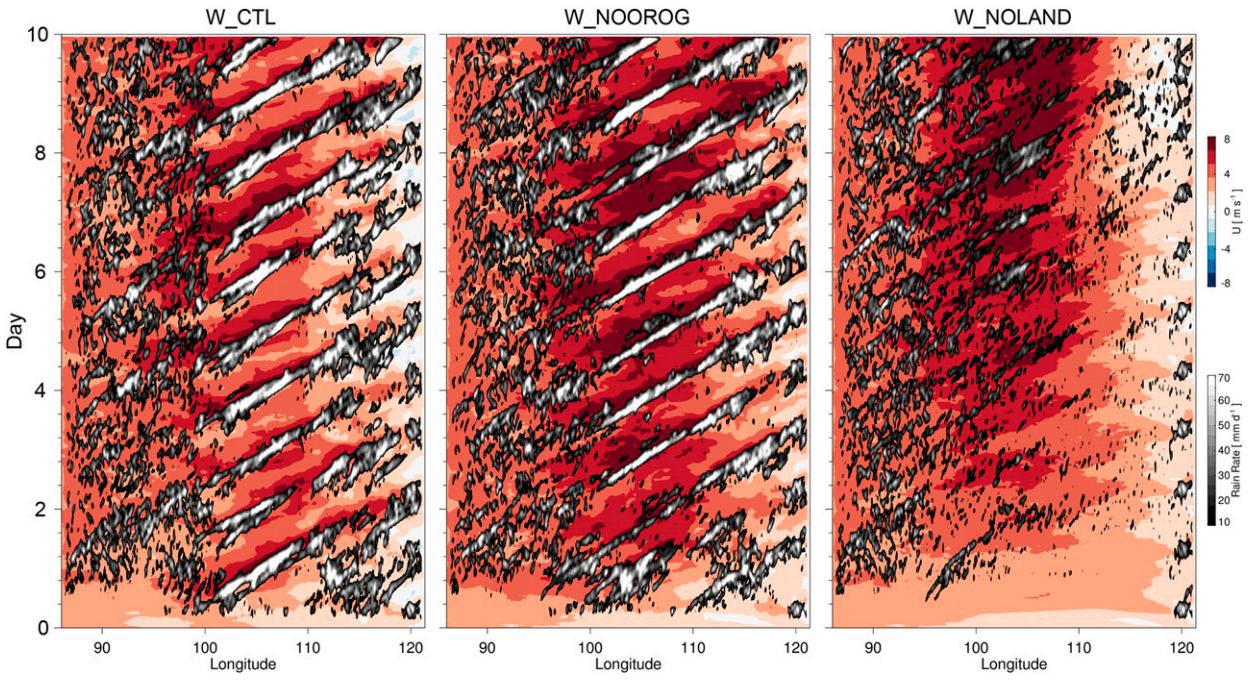

FIG. 7. As in Fig. 3, but for the simulations conducted using the westerly wind regime composite.

convection later intensifies around 1900 LT, propagation appears to effectively restart from this longitude and time. Flattening orography effectively removes this discontinuity in W_NOOROG (Fig. 8). Although convection develops over Sumatra around the same time (~1900 LT), its subsequent eastward propagation is continuous across Borneo, owing to diurnal convection being delayed there by ~6 h as compared to W_CTL. These results imply that the mountain range of central Borneo (Fig. 1) exerts a strong control over the diurnal timing of rainfall there in this flow regime. These results also imply that when the phase speed does not perfectly match the diurnal phase-locking phase speed of ~17–18 m s^{-1} (given the Borneo–Sumatra separation of ~1500 km), the diurnal gravity wave propagation may be disrupted by local diurnal convective forcing.

While it is difficult to identify the exact cause for the slower phase speed in W_CTL as compared to CTL (Figs. 4 and 8), the flow regimes are very distinct, with the westerly regime having much stronger vertical shear due to the flow reversal from low to upper levels (Fig. 2). While we do not yet fully understand the cause for this distinction, we may nevertheless further examine the nature of these modes.

Cross sections are provided for W_CTL in Fig. 9, which are analogous to those provided for CTL (Fig. 6). One clear difference of the deep convection here as compared to CTL is a prominent westward tilt with height, which likely owes to the strongly sheared zonal flow pattern (Figs. 2 and 9a). In addition, convection is more bottom-heavy than that in CTL, especially that originating in Sumatra, which is characterized by peaks in w maximizing from ~300 to 500 hPa. This implies a lower fraction of stratiform rainfall and greater proportion of convection in the westerly regime. Yet, in other senses there are many parallels between the regimes. As in CTL, the convective systems propagate slower (~11 m s^{-1}) than the overriding gravity wave manifest in u' and θ_v^*. Furthermore, as in CTL, the cross sections reveal prominent upward- and downward-tilted rays in u' and θ_v^* that radiate eastward from (ahead of) a source in the upper troposphere (Figs. 6b,c). These quadrature signatures are indicative of gravity wave energy excited by an eastward-moving heat source, consistent with the results from CTL.

Comparing the tests W_CTL, W_NOOROG, and W_NOLAND supports the conclusions drawn from the easterly regime (Figs. 7 and 8). Namely, to first order, the diurnal gravity waves are similar in character both with and without orography, while the removal of land fully removes the diurnal propagating signal. W_NOLAND does exhibit propagating modes that are prominent in comparison with NOLAND, albeit without diurnal phasing (Figs. 4, 8, and 9). Greater rainfall in W_NOLAND than in NOLAND is consistent with more moist conditions in the former due to the MJO active phase (Fig. 2). One distinction

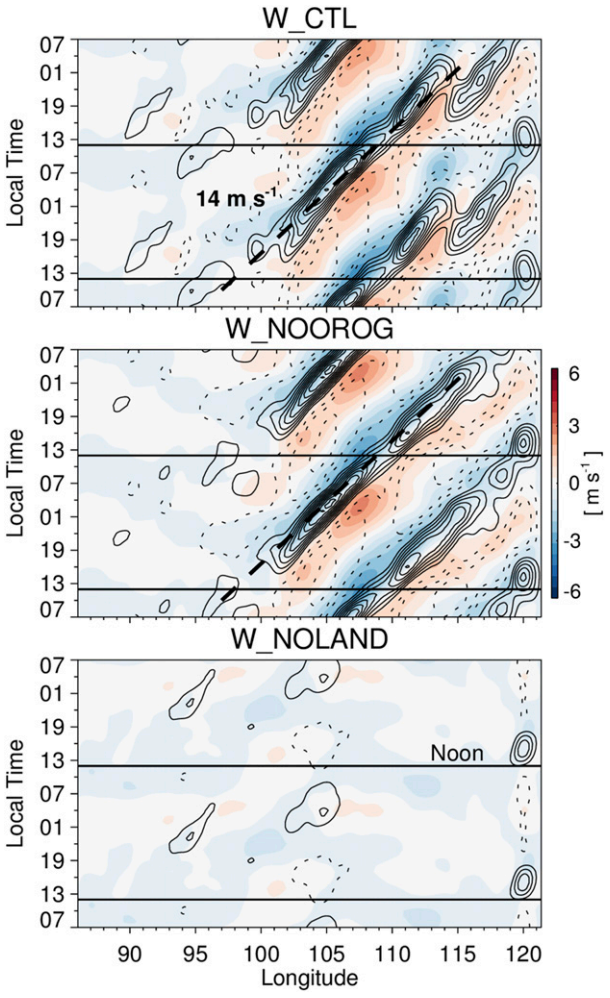

FIG. 8. As in Fig. 4, but for the simulations conducted using the westerly wind regime composite, and with u' at 400 hPa. Phase speed lines of 14 m s^{-1} (black dashed) are depicted.

between the westerly and easterly regimes, as noted earlier, is that the gravity waves of the westerly regime appear to be discontinuous in time across Borneo with orography included and more continuous without it (Fig. 8). This impact implies that the mountain range of central Borneo strongly controls the diurnal triggering of rainfall; with this orography removed, the gravity wave more strongly governs rainfall timing.

The overall results of both the easterly regime and westerly regime indicate that orography plays a secondary role to the diurnal gravity waves of the MC. Orography modulates details of these gravity waves, such as the relative amount of offshore rainfall and the exact timing of inland convective initiation (Figs. 4 and 8). Yet, it appears to not be vital to either the existence of these waves or their phase speed. We therefore conclude that latent heating from organized moist convection is more critical to exciting and maintaining these waves (Raymond 1984; Tripoli and Cotton 1989; RZ19).

b. *Impact of synchronized diurnal forcing of Borneo and Sumatra*

In this section we discuss the potential feedback exerted on the diurnal gravity waves by the synchronized diurnal forcing of Sumatra and Borneo using the easterly composite. RZ19 hypothesized that the synchronized diurnal MCS activity in the two island regions results in a stronger diurnal gravity wave response than would otherwise occur. The model tests CTL, NOLAND, NOBORN, and NOSUM are invoked to test this hypothesis. Factor separation is used to isolate the nonlinear interaction between the two islands. We seek to isolate the distinct impacts of the two islands, which hence serve as two independent factors. We require $2^n = 4$ separate simulations to isolate these factors, where n is the number of factors (Stein and Alpert 1993). The nonlinear forcing can therefore be written as $f_{\mathrm{NL}} = f_{12} - (f_1 + f_2) + f_0$, where f_0 excludes both factors (i.e., NOLAND), f_1 (NOBORN), and f_2 (NOSUM) are the individual factors, and f_{12} includes both factors (CTL). We may also write $f_L = f_1 + f_2 - f_0$, where f_L is the linear sum of the two factors.

The results of this factor separation are depicted in Fig. 10, which displays diurnal composites (as in Fig. 4) for the different factor terms. To first order, the diurnally forced gravity wave response to each island, sums linearly to form the pattern of CTL, as depicted in f_L. A systematic pattern in f_{NL} is apparent, however: the wave signature in upper-level u' is amplified and/or phase shifted later in time by ~3 h directly between the two main MCS forcing regions of the two islands, that is, from ~102° to 110°E. Weak amplification of this signal is apparent in positive u' anomalies across most of Sumatra and its immediate offshore region, that is, out to ~93°E. Several isolated regions of rainfall indicate an associated intensification of rainfall in f_{NL}: that is, a center near 105°E, one from 100° to 103°E, and a broader one from ~93° to 99°E. While these rainfall anomalies are difficult to interpret individually, taken together with the more contiguous associated u' signature, they suggest a minor amplification of the diurnal gravity wave. The large-magnitude rainfall anomalies near the western edge of the domain are difficult to explain, and may be influenced by spurious domain edge effects, such as reflection.

These findings support the hypothesis that the synchronized diurnal forcing of Borneo and Sumatra amplifies the diurnal gravity wave signal, compared to if either island existed in isolation. More generally, this

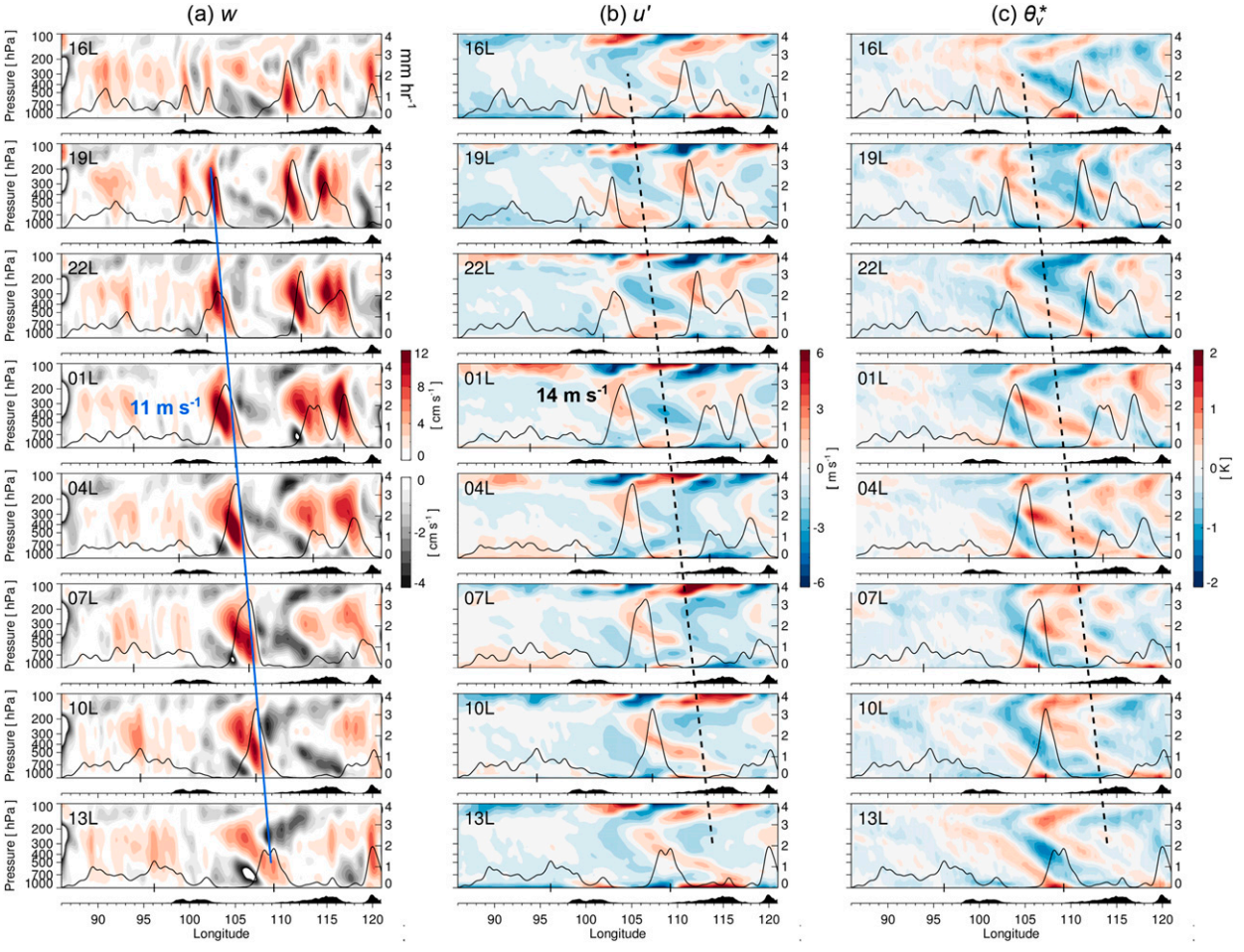

FIG. 9. As in Fig. 6, but for the simulation W_CTL. Phase speed lines of 11 (blue solid) and 14 m s^{-1} (black dashed) are depicted.

indicates that islands within a certain proximity of one another are modulated by the diurnal circulation forcing from their neighboring islands, which in turn influences diurnal rainfall signatures. Yet, this effect appears to be secondary, at most, to the linear sum of the gravity waves forced by the two islands individually.

4. Summary and conclusions

The Maritime Continent (MC) is characterized by very prominent, long-lived diurnal rainfall disturbances that propagate zonally across multiple islands and span multiple days (Ichikawa and Yasunari 2007). A recent study by RZ19 suggests that these disturbances can be explained as diurnally phase-locked gravity waves. The present study has investigated the dynamics and origins of these gravity waves through a set of regional cloud-permitting model experiments that invoke diurnally cyclic lateral boundary conditions and realistic geography. We have conducted experiments for two regimes: 1) an easterly flow regime characteristic of the MJO suppressed phase in the MC, and 2) a westerly regime characteristic of the MJO active phase in the MC. These regimes are characterized by westward- and eastward-propagating diurnal waves, respectively.

The origins and nature of these gravity waves have been investigated through sensitivity tests either with the orography of Borneo and/or Sumatra removed or with the islands removed in entirety. These tests demonstrate that the diurnal gravity waves owe their existence to latent heating from the vigorous nocturnal mesoscale convective systems (MCSs) that form in both Borneo and Sumatra. We have also found that while orography may influence the evolution of the MCSs, it is not critical to the existence of the diurnal gravity waves.

These gravity waves are diurnally phase-locked, meaning that they propagate the distance between Borneo and Sumatra in approximately 24 h (RZ19). Given this phasing, they couple with the diurnal cycle of deep organized convection in both Borneo and

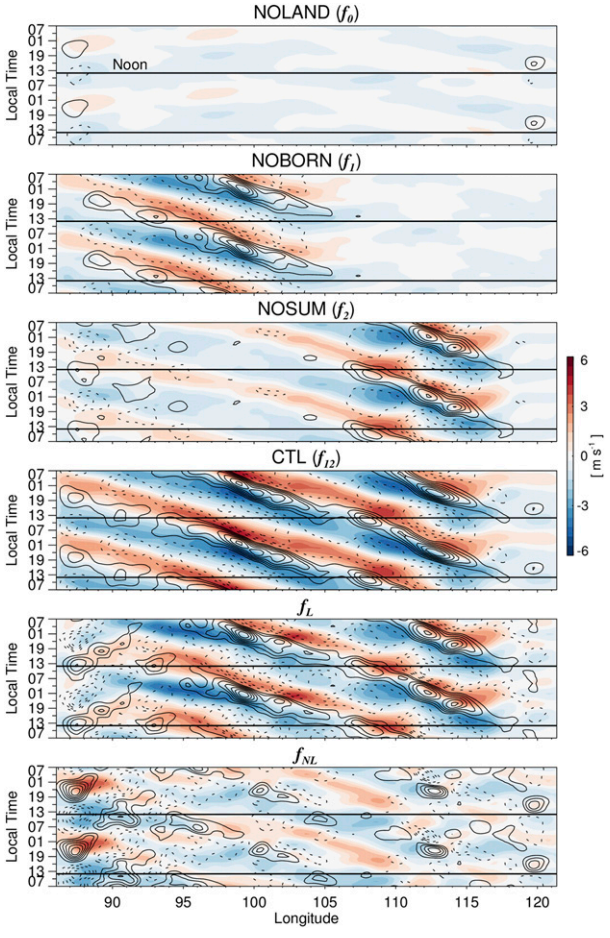

FIG. 10. As in Fig. 4, but for factor separation assessment of nonlinear feedback between Borneo and Sumatra, with (top to bottom) NOLAND (f_0), NOBORN (f_1), NOSUM (f_2), CTL (f_{12}), the linear sum (f_L), and the residual due to nonlinear interaction f_{NL}.

Sumatra. RZ19 hypothesized that the synchronized diurnal forcing of Borneo and Sumatra promotes a stronger gravity wave response compared to if the islands existed in isolation. The results of factor separation indicate that nonlinear interaction of these two islands' diurnal cycles indeed slightly amplifies this gravity wave mode, especially at longitude between the two islands. This nonlinear component is a small-order effect, however, and therefore, the propagating gravity wave mode in this case can be represented to first order by the linear sum of the responses to each island as simulated in isolation.

The overall conclusion of this study is that latent heating from deep convection is vital to both exciting and maintaining the zonally propagating diurnal gravity waves of the MC. Further study is required to determine whether or not these findings apply for offshore-propagating diurnal rainfall systems in other regions, or for nocturnal propagating convection in continental regimes downstream of major mountain chains. To this end, we suggest the following hypothesis that future studies may examine: diurnal gravity waves and their associated coupled rainfall signatures are driven by latent heating due to vigorous organized convection, and are only sensitive to orography to the extent that the deep convection is triggered by or modulated by orographic flows.

Acknowledgments. We acknowledge support for this research from the National Science Foundation through Grant 1712290 and the Office of Science of the Department of Energy Grant WACCEM (Water Cycle and Climate Extremes Modeling) subcontracted through PNNL (Pacific Northwest National Laboratory). We are very grateful to George Kiladis and an anonymous reviewer for their helpful comments on the study. We also acknowledge the Texas Advanced Computing Center (TACC) at the University of Texas at Austin (http://www.tacc.utexas.edu) for computational resources invoked in this research.

REFERENCES

Aves, S., and R. H. Johnson, 2008: The diurnal cycle of convection over the northern South China Sea. *J. Meteor. Soc. Japan*, **86**, 919–934, https://doi.org/10.2151/jmsj.86.919.

Bao, X., and F. Zhang, 2013: Impacts of the mountain–plains solenoid and cold pool dynamics on the diurnal variation of warm-season precipitation over northern China. *Atmos. Chem. Phys.*, **13**, 6965–6982, https://doi.org/10.5194/acp-13-6965-2013.

——, ——, and J. Sun, 2011: Diurnal variations of warm-season precipitation east of the Tibetan Plateau over China. *Mon. Wea. Rev.*, **139**, 2790–2810, https://doi.org/10.1175/MWR-D-11-00006.1.

Carbone, R. E., and J. D. Tuttle, 2008: Rainfall occurrence in the U.S. warm season: The diurnal cycle. *J. Climate*, **21**, 4132–4146, https://doi.org/10.1175/2008JCLI2275.1.

——, J. W. Wilson, T. D. Keenan, and J. M. Hacker, 2000: Tropical island convection in the absence of significant topography. Part I: Life cycle of diurnally forced convection. *Mon. Wea. Rev.*, **128**, 3459–3480, https://doi.org/10.1175/1520-0493(2000)128<3459:TICITA>2.0.CO;2.

——, J. D. Tuttle, D. A. Ahijevych, and S. B. Trier, 2002: Inferences of predictability associated with warm season precipitation episodes. *J. Atmos. Sci.*, **59**, 2033–2056, https://doi.org/10.1175/1520-0469(2002)059<2033:IOPAWW>2.0.CO;2.

Chen, X., and F. Zhang, 2019: Relative roles of preconditioning moistening and global circumnavigating mode on the MJO convective initiation during DYNAMO. *Geophys. Res. Lett.*, **46**, 1079–1087, https://doi.org/10.1029/2018GL080987.

——, ——, and K. Zhao, 2016: Diurnal variations of the land–sea breeze and its related precipitation over South China. *J. Atmos. Sci.*, **73**, 4793–4815, https://doi.org/10.1175/JAS-D-16-0106.1.

——, ——, and ——, 2017: Influence of monsoonal wind speed and moisture content on intensity and diurnal variations of the mei-yu season coastal rainfall over South China. *J. Atmos. Sci.*, **74**, 2835–2856, https://doi.org/10.1175/JAS-D-17-0081.1.

——, O. M. Pauluis, and F. Zhang, 2018: Atmospheric overturning across multiple scales of an MJO event during the CINDY/DYNAMO campaign. *J. Atmos. Sci.*, **75**, 381–399, https://doi.org/10.1175/JAS-D-17-0060.1.

Chou, M.-D., and M. J. Suarez, 1994: An efficient thermal infrared radiation parameterization for use in general circulation models. NASA Tech. Memo. 104606, Vol. 3, 85 pp., https://archive.org/details/nasa_techdoc_19950009331.

Coppin, D., and G. Bellon, 2019: Physical mechanisms controlling the offshore propagation of convection in the tropics: 1. Flat island. *J. Adv. Model. Earth Syst.*, **11**, 3042–3056, https://doi.org/10.1029/2019MS001793.

Cronin, T. W., 2014: On the choice of average solar zenith angle. *J. Atmos. Sci.*, **71**, 2994–3003, https://doi.org/10.1175/JAS-D-13-0392.1.

——, K. A. Emanuel, and P. Molnar, 2015: Island precipitation enhancement and the diurnal cycle in radiative-convective equilibrium. *Quart. J. Roy. Meteor. Soc.*, **141**, 1017–1034, https://doi.org/10.1002/QJ.2443.

Dai, A., 2001: Global precipitation and thunderstorm frequencies. Part II: Diurnal variations. *J. Climate*, **14**, 1112–1128, https://doi.org/10.1175/1520-0442(2001)014<1112:GPATFP>2.0.CO;2.

Dee, D. P., and Coauthors, 2011: The ERA-Interim reanalysis: Configuration and performance of the data assimilation system. *Quart. J. Roy. Meteor. Soc.*, **137**, 553–597, https://doi.org/10.1002/QJ.828.

Feng, J., T. Li, and W. Zhu, 2015: Propagating and nonpropagating MJO events over Maritime Continent. *J. Climate*, **28**, 8430–8449, https://doi.org/10.1175/JCLI-D-15-0085.1.

Fovell, R., G. Mullendore, and S. Kim, 2006: Discrete propagation in numerically simulated nocturnal squall lines. *Mon. Wea. Rev.*, **134**, 3735–3752, https://doi.org/10.1175/MWR3268.1.

Fujita, M., K. Yuneyama, S. Mori, T. Nasuno, and M. Satoh, 2011: Diurnal convection peaks over the eastern Indian Ocean off Sumatra during different MJO phases. *J. Meteor. Soc. Japan*, **89A**, 317–330, https://doi.org/10.2151/jmsj.2011-A22.

Gonzalez, A. O., and X. Jiang, 2017: Winter mean lower tropospheric moisture over the Maritime Continent as a climate model diagnostic metric for the propagation of the Madden-Julian oscillation. *Geophys. Res. Lett.*, **44**, 2588–2596, https://doi.org/10.1002/2016GL072430.

Gray, W. M., and R. W. Jacobson, 1977: Diurnal variation of deep cumulus convection. *Mon. Wea. Rev.*, **105**, 1171–1188, https://doi.org/10.1175/1520-0493(1977)105<1171:DVODCC>2.0.CO;2.

Hagos, S. M., C. Zhang, Z. Feng, C. D. Burleyson, C. De Mott, B. Kerns, J. J. Benedict, and M. N. Martini, 2016: The impact of the diurnal cycle on the propagation of Madden-Julian oscillation convection across the Maritime Continent. *J. Adv. Model. Earth Syst.*, **8**, 1552–1564, https://doi.org/10.1002/2016MS000725.

Houze, R. A., Jr., S. G. Geotis, F. D. Marks, and A. K. West, 1981: Winter monsoon convection in the vicinity of North Borneo. Part I: Structure and time variation of the clouds and precipitation. *Mon. Wea. Rev.*, **109**, 1595–1614, https://doi.org/10.1175/1520-0493(1981)109<1595:WMCITV>2.0.CO;2.

Huang, H.-L., C.-C. Wang, G. T.-J. Chen, and R. E. Carbone, 2010: The role of diurnal solenoidal circulation on propagating rainfall episodes near the eastern Tibetan Plateau. *Mon. Wea. Rev.*, **138**, 2975–2989, https://doi.org/10.1175/2010MWR3225.1.

Iacono, M. J., J. S. Delamere, E. J. Mlawer, M. W. Shephard, S. A. Clough, and W. D. Collins, 2008: Radiative forcing by long-lived greenhouse gases: Calculations with the AER radiative transfer models. *J. Geophys. Res.*, **113**, D13103, https://doi.org/10.1029/2008JD009944.

Ichikawa, H., and T. Yasunari, 2006: Time–space characteristics of diurnal rainfall over Borneo and surrounding oceans as observed by TRMM-PR. *J. Climate*, **19**, 1238–1260, https://doi.org/10.1175/JCLI3714.1.

——, and ——, 2007: Propagating diurnal disturbances embedded in the Madden-Julian oscillation. *Geophys. Res. Lett.*, **34**, L18811, https://doi.org/10.1029/2007GL030480.

——, and ——, 2008: Intraseasonal variability in diurnal rainfall over New Guinea and the surrounding oceans during austral summer. *J. Climate*, **21**, 2852–2868, https://doi.org/10.1175/2007JCLI1784.1.

Johnson, R. H., 1982: Vertical motion in near-equatorial winter monsoon convection. *J. Meteor. Soc. Japan*, **60**, 682–690, https://doi.org/10.2151/JMSJ1965.60.2_682.

——, 2011: Diurnal cycle of monsoon convection. *The Global Monsoon System: Research and Forecast*, C. P. Chang et al., Eds., World Scientific, 257–276.

——, and D. L. Priegnitz, 1981: Winter monsoon convection in the vicinity of North Borneo. Part II: Effects on large-scale fields. *Mon. Wea. Rev.*, **109**, 1615–1628, https://doi.org/10.1175/1520-0493(1981)109<1615:WMCITV>2.0.CO;2.

——, and D. C. Kriete, 1982: Thermodynamic and circulation characteristics of winter monsoon tropical mesoscale convection. *Mon. Wea. Rev.*, **110**, 1898–1911, https://doi.org/10.1175/1520-0493(1982)110<1898:TACCOW>2.0.CO;2.

——, and J. F. Bresch, 1991: Diagnosed characteristics of precipitation systems over Taiwan during the May–June 1987 TAMEX. *Mon. Wea. Rev.*, **119**, 2540–2557, https://doi.org/10.1175/1520-0493(1991)119<2540:DCOPSO>2.0.CO;2.

Kikuchi, K., and B. Wang, 2008: Diurnal precipitation regimes in the global tropics. *J. Climate*, **21**, 2680–2696, https://doi.org/10.1175/2007JCLI2051.1.

Kiladis, G. N., M. C. Wheeler, P. T. Haertel, K. H. Straub, and P. E. Roundy, 2009: Convectively coupled equatorial waves. *Rev. Geophys.*, **47**, RG2003, https://doi.org/10.1029/2008RG000266.

Kuang, Z., 2008: A moisture-stratiform instability for convectively coupled waves. *J. Atmos. Sci.*, **65**, 834–854, https://doi.org/10.1175/2007JAS2444.1.

Laing, A. G., R. Carbone, V. Levizzani, and J. Tuttle, 2008: The propagation and diurnal cycles of deep convection in northern tropical Africa. *Quart. J. Roy. Meteor. Soc.*, **134**, 93–109, https://doi.org/10.1002/QJ.194.

Ling, J., C. Zhang, R. Joyce, P. Xie, and G. Chen, 2019: Possible role of the diurnal cycle in land convection in the barrier effect on the MJO by the Maritime Continent. *Geophys. Res. Lett.*, **46**, 3001–3011, https://doi.org/10.1029/2019GL081962.

Love, B. S., A. J. Matthews, and G. M. S. Lister, 2011: The diurnal cycle of precipitation over the Maritime Continent in a high-resolution atmospheric model. *Quart. J. Roy. Meteor. Soc.*, **137**, 934–947, https://doi.org/10.1002/QJ.809.

Madden, R. A., and P. R. Julian, 1972: Description of global-scale circulation cells in the tropics with a 40–50 day period. *J. Atmos. Sci.*, **29**, 1109–1123, https://doi.org/10.1175/1520-0469(1972)029<1109:DOGSCC>2.0.CO;2.

Mapes, B. E., 1993: Gregarious tropical convection. *J. Atmos. Sci.*, **50**, 2026–2037, https://doi.org/10.1175/1520-0469(1993)050<2026:GTC>2.0.CO;2.

——, 2000: Convective inhibition, subgrid-scale triggering energy, and stratiform instability in a toy tropical wave model. *J. Atmos. Sci.*, **57**, 1515–1535, https://doi.org/10.1175/1520-0469(2000)057<1515:CISSTE>2.0.CO;2.

——, and R. A. Houze Jr., 1993: Cloud clusters and superclusters over the oceanic warm pool. *Mon. Wea. Rev.*, **121**, 1398–1416, https://doi.org/10.1175/1520-0493(1993)121<1398:CCASOT>2.0.CO;2.

——, T. T. Warner, M. Xu, and A. J. Negri, 2003a: Diurnal patterns of rainfall in northwestern South America. Part I: Observations and context. *Mon. Wea. Rev.*, **131**, 799–812, https://doi.org/10.1175/1520-0493(2003)131<0799:DPORIN>2.0.CO;2.

——, ——, and ——, 2003b: Diurnal patterns of rainfall in northwestern South America. Part III: Diurnal gravity waves and nocturnal convection offshore. *Mon. Wea. Rev.*, **131**, 830–844, https://doi.org/10.1175/1520-0493(2003)131<0830:DPORIN>2.0.CO;2.

——, S. Tulich, J. Lin, and P. Zuidema, 2006: The mesoscale convection life cycle: Building block or prototype for large-scale tropical waves? *Dyn. Atmos. Oceans*, **42**, 3–29, https://doi.org/10.1016/j.dynatmoce.2006.03.003.

Markowski, P., and Y. Richardson, 2010: *Mesoscale Meteorology in Midlatitudes*. John Wiley and Sons, 430 pp.

Mori, S., and Coauthors, 2004: Diurnal land–sea rainfall peak migration over Sumatera Island, Indonesian Maritime Continent, observed by TRMM satellite and intensive rawinsonde soundings. *Mon. Wea. Rev.*, **132**, 2021–2039, https://doi.org/10.1175/1520-0493(2004)132<2021:DLRPMO>2.0.CO;2.

Neale, R., and J. Slingo, 2003: The Maritime Continent and its role in the global climate: A GCM study. *J. Climate*, **16**, 834–848, https://doi.org/10.1175/1520-0442(2003)016<0834:TMCAIR>2.0.CO;2.

Nesbitt, S. W., and E. J. Zipser, 2003: The diurnal cycle of rainfall and convective intensity according to three years of TRMM measurements. *J. Climate*, **16**, 1456–1475, https://doi.org/10.1175/1520-0442-16.10.1456.

Nicholls, M. E., R. A. Pielke, and W. R. Cotton, 1991: Thermally forced gravity waves in an atmosphere at rest. *J. Atmos. Sci.*, **48**, 1869–1884, https://doi.org/10.1175/1520-0469(1991)048<1869:TFGWIA>2.0.CO;2.

Oh, J.-H., K.-Y. Kim, and G.-H. Lim, 2012: Impact of MJO on the diurnal cycle of rainfall over the western Maritime Continent in the austral summer. *Climate Dyn.*, **38**, 1167–1180, https://doi.org/10.1007/s00382-011-1237-4.

Ohsawa, T., H. Ueda, T. Hayashi, A. Watanabe, and J. Matsumoto, 2001: Diurnal variations of convective activity and rainfall in tropical Asia. *J. Meteor. Soc. Japan*, **79**, 333–352, https://doi.org/10.2151/jmsj.79.333.

Pritchard, M. S., M. W. Moncrieff, and R. C. J. Somerville, 2011: Orogenic propagating precipitation systems over the United States in a global climate model with embedded explicit convection. *J. Atmos. Sci.*, **68**, 1821–1840, https://doi.org/10.1175/2011JAS3699.1.

Qian, J.-H., 2008: Why precipitation is mostly concentrated over islands in the Maritime Continent. *J. Atmos. Sci.*, **65**, 1428–1441, https://doi.org/10.1175/2007JAS2422.1.

Qian, T., C. C. Epifanio, and F. Zhang, 2012: Topographic effects on the tropical land and sea breeze. *J. Atmos. Sci.*, **69**, 130–149, https://doi.org/10.1175/JAS-D-11-011.1.

Randall, D. A., Harshvardhan, and D. A. Dazlich, 1991: Diurnal variability of the hydrologic cycle in a general circulation model. *J. Atmos. Sci.*, **48**, 40–62, https://doi.org/10.1175/1520-0469(1991)048<0040:DVOTHC>2.0.CO;2.

Raymond, D. J., 1984: A wave-CISK model of squall lines. *J. Atmos. Sci.*, **41**, 1946–1958, https://doi.org/10.1175/1520-0469(1984)041<1946:AWCMOS>2.0.CO;2.

Ruppert, J. H., 2016: Diurnal timescale feedbacks in the tropical cumulus regime. *J. Adv. Model. Earth Syst.*, **8**, 1483–1500, https://doi.org/10.1002/2016MS000713.

——, and R. H. Johnson, 2016: On the cumulus diurnal cycle over the tropical warm pool. *J. Adv. Model. Earth Syst.*, **8**, 669–690, https://doi.org/10.1002/2015MS000610.

——, and C. Hohenegger, 2018: Diurnal circulation adjustment and organized deep convection. *J. Climate*, **31**, 4899–4916, https://doi.org/10.1175/JCLI-D-17-0693.1.

——, and F. Zhang, 2019: Diurnal forcing and phase locking of gravity waves in the Maritime Continent. *J. Atmos. Sci.*, **76**, 2815–2835, https://doi.org/10.1175/JAS-D-19-0061.1.

——, and X. Chen, 2020: Island rainfall enhancement in the Maritime Continent. *Geophys. Res. Lett.*, https://doi.org/10.1029/2019GL086545, in press.

——, R. H. Johnson, and A. K. Rowe, 2013: Diurnal circulations and rainfall in Taiwan during SoWMEX/TiMREX (2008). *Mon. Wea. Rev.*, **141**, 3851–3872, https://doi.org/10.1175/MWR-D-12-00301.1.

Sakaeda, N., G. Kiladis, and J. Dias, 2017: The diurnal cycle of tropical cloudiness and rainfall associated with the Madden–Julian oscillation. *J. Climate*, **30**, 3999–4020, https://doi.org/10.1175/JCLI-D-16-0788.1.

Sakurai, N., and Coauthors, 2009: Internal structures of migratory cloud systems with diurnal cycle over Sumatera Island during CPEA-I campaign. *J. Meteor. Soc. Japan*, **87**, 157–170, https://doi.org/10.2151/jmsj.87.157.

Shi, J. J., and Coauthors, 2010: WRF simulations of the 20–22 January 2007 snow events over eastern Canada: Comparison with in situ and satellite observations. *J. Appl. Meteor. Climatol.*, **49**, 2246–2266, https://doi.org/10.1175/2010JAMC2282.1.

Skamarock, W. C., and Coauthors, 2008: A description of the Advanced Research WRF version 3. NCAR Tech. Note NCAR/TN-475+STR, 113 pp., http://doi.org/10.5065/D68S4MVH.

Stein, U., and P. Alpert, 1993: Factor separation in numerical simulations. *J. Atmos. Sci.*, **50**, 2107–2115, https://doi.org/10.1175/1520-0469(1993)050<2107:FSINS>2.0.CO;2.

Stensrud, D. J., 1996: Importance of low-level jets to climate: A review. *J. Climate*, **9**, 1698–1711, https://doi.org/10.1175/1520-0442(1996)009<1698:IOLLJT>2.0.CO;2.

Sun, J., and F. Zhang, 2012: Impacts of mountain–plains solenoid on diurnal variations of rainfalls along the mei-yu front over the East China plains. *Mon. Wea. Rev.*, **140**, 379–397, https://doi.org/10.1175/MWR-D-11-00041.1.

Takayabu, Y. N., K.-M. Lau, and C.-H. Sui, 1996: Observation of a quasi-2-day wave during TOGA COARE. *Mon. Wea. Rev.*, **124**, 1892–1913, https://doi.org/10.1175/1520-0493(1996)124<1892:OOAQDW>2.0.CO;2.

Trier, S. B., C. A. Davis, and D. Ahijevych, 2010: Environmental controls on the simulated diurnal cycle of warm-season precipitation in the continental United States. *J. Atmos. Sci.*, **67**, 1066–1090, https://doi.org/10.1175/2009JAS3247.1.

——, ——, and R. E. Carbone, 2014: Mechanisms governing the persistence and diurnal cycle of a heavy rainfall corridor. *J. Atmos. Sci.*, **71**, 4102–4126, https://doi.org/10.1175/JAS-D-14-0134.1.

Tripoli, G. J., and W. R. Cotton, 1989: Numerical study of an observed orogenic mesoscale convective system. Part 2: Analysis of governing dynamics. *Mon. Wea. Rev.*, **117**, 305–328, https://doi.org/10.1175/1520-0493(1989)117<0305:NSOAOO>2.0.CO;2.

Tulich, S. N., and B. E. Mapes, 2008: Multiscale convective wave disturbances in the tropics: Insights from a two-dimensional cloud-resolving model. *J. Atmos. Sci.*, **65**, 140–155, https://doi.org/10.1175/2007JAS2353.1.

——, D. A. Randall, and B. E. Mapes, 2007: Vertical-mode and cloud decomposition of large-scale convectively coupled gravity waves in a two-dimensional cloud-resolving model. *J. Atmos. Sci.*, **64**, 1210–1229, https://doi.org/10.1175/JAS3884.1.

Vincent, C. L., and T. P. Lane, 2016: Evolution of the diurnal precipitation cycle with the passage of a Madden–Julian oscillation event through the Maritime Continent. *Mon. Wea. Rev.*, **144**, 1983–2005, https://doi.org/10.1175/MWR-D-15-0326.1.

Wang, C.-C., G. T.-J. Chen, and R. E. Carbone, 2004: A climatology of warm-season cloud patterns over East Asia based on GMS infrared brightness temperature observations. *Mon. Wea. Rev.*, **132**, 1606–1629, https://doi.org/10.1175/1520-0493(2004)132<1606:ACOWCP>2.0.CO;2.

Wang, S., A. H. Sobel, F. Zhang, Y. Q. Sun, Y. Yue, and L. Zhou, 2015: Regional simulation of the October and November MJO events observed during the CINDY/DYNAMO field campaign at gray zone resolution. *J. Climate*, **28**, 2097–2119, https://doi.org/10.1175/JCLI-D-14-00294.1.

Warner, T. T., B. E. Mapes, and M. Xu, 2003: Diurnal patterns of rainfall in northwestern South America. Part II: Model simulations. *Mon. Wea. Rev.*, **131**, 813–829, https://doi.org/10.1175/1520-0493(2003)131<0813:DPORIN>2.0.CO;2.

Yamanaka, M. D., S.-Y. Ogino, P.-M. Wu, H. Jun-Ichi, S. Mori, J. Matsumoto, and F. Syamsudin, 2018: Maritime Continent coastlines controlling Earth's climate. *Prog. Earth Planet. Sci.*, **5**, 21, https://doi.org/10.1186/s40645-018-0174-9.

Yang, G.-Y., and J. Slingo, 2001: The diurnal cycle in the tropics. *Mon. Wea. Rev.*, **129**, 784–801, https://doi.org/10.1175/1520-0493(2001)129<0784:TDCITT>2.0.CO;2.

Yang, S., and E. A. Smith, 2006: Mechanisms for diurnal variability of global tropical rainfall observed from TRMM. *J. Climate*, **19**, 5190–5226, https://doi.org/10.1175/JCLI3883.1.

Ying, Y., and F. Zhang, 2017: Practical and intrinsic predictability of multiscale weather and convectively coupled equatorial waves during the active phase of an MJO. *J. Atmos. Sci.*, **74**, 3771–3785, https://doi.org/10.1175/JAS-D-17-0157.1.

Yoneyama, K., C. Zhang, and C. N. Long, 2013: Tracking pulses of the Madden–Julian oscillation. *Bull. Amer. Meteor. Soc.*, **94**, 1871–1891, https://doi.org/10.1175/BAMS-D-12-00157.1.

Zeng, X., and A. Beljaars, 2005: A prognostic scheme of sea surface skin temperature for modeling and data assimilation. *Geophys. Res. Lett.*, **32**, L14605, https://doi.org/10.1029/2005GL023030.

Zhang, C., and J. Ling, 2017: Barrier effect of the Indo-Pacific Maritime Continent on the MJO: Perspectives from tracking MJO precipitation. *J. Climate*, **30**, 3439–3459, https://doi.org/10.1175/JCLI-D-16-0614.1.

Zhang, F., S. Taraphdar, and S. Wang, 2017: The role of global circumnavigating mode in the MJO initiation and propagation. *J. Geophys. Res. Atmos.*, **122**, 5837–5856, https://doi.org/10.1002/2016JD025665.

Zhang, Y., F. Zhang, C. A. Davis, and J. Sun, 2018: Diurnal evolution and structure of long-lived mesoscale convective vortices along the mei-yu front over the East China plains. *J. Atmos. Sci.*, **75**, 1005–1025, https://doi.org/10.1175/JAS-D-17-0197.1.

Zuidema, P., 2003: Convective clouds over the Bay of Bengal. *Mon. Wea. Rev.*, **131**, 780–798, https://doi.org/10.1175/1520-0493(2003)131<0780:CCOTBO>2.0.CO;2.